Astron. Astrophys. 310, 613–628 (1996)

ASTRONOMY AND ASTROPHYSICS

Spectral analysis of the multiple-shell planetary nebula LoTr 4 and its very hot hydrogen-deficient central star*

T. Rauch[1], J. Köppen[1,2], and K. Werner[1,3]

[1] Institut für Astronomie und Astrophysik der Universität, D-24098 Kiel, Germany (e-mail: rauch@astrophysik.uni-kiel.de)
[2] URA1280, Observatoire Astronomique, 11, rue de l'université, F-67000 Strasbourg, France
[3] Lehrstuhl Astrophysik, Universität Potsdam, Am Neuen Palais 10, D-14469 Potsdam, Germany

Received 10 August 1995 / Accepted 28 October 1995

Abstract. We present a spectral analysis of the planetary nebula LoTr 4 and its exciting star and report the discovery of a multiple-shell nebula structure.

Two clearly separated shells can be detected around the central star with radii of 7.5″ and 13.5″ with a strong decrease of brightness from south-east to north-west. Relative to these shells the central star appears to be off-centered by about 2″ to the south-east. A fragment of a third shell is found with a radius of 22.5″ south-east of the central star. This and the high degree of asymmetry indicate that the nebula ejection was a complicated process.

LoTr 4 is of high excitation with a geometrical radius of $r = 0.6^{+0.2}_{-0.3}$ pc and a mass of $M = 0.29\,M_{\odot}$. Its helium abundance is definitely solar (±0.05dex), while the trace elements could also have slightly different abundances (±0.1dex). A stratification of the He/H abundance ratio in the nebula can be excluded.

The central star had been analyzed by means of NLTE model atmospheres. From line profile fits we derive an effective temperature of $T_{\rm eff} = 120 \pm 15$kK and a surface gravity of $\log g = 5.5 \pm 0.3$. The photosphere is dominated by helium and hydrogen ($n_{\rm H}/n_{\rm He} =$ 0.5 by number). We find a solar nitrogen abundance ($n_{\rm N}/n_{\rm He} = 0.001$). Neither carbon nor oxygen lines are exhibited in its spectrum which sets the upper limits to $n_{\rm C}/n_{\rm He} < 0.004$ and $n_{\rm O}/n_{\rm He} < 0.008$ which are the solar abundance ratios.

These abundances indicate that the central star of LoTr 4 can be a "born-again post-AGB star". This scenario has also been invoked for the evolution of PG 1159 stars. In this picture the O(He) stars, LoTr 4 and K 1-27, might either be direct progenitors of the PG 1159 stars or they have experienced less drastic mass-loss events.

Key words: stars: abundances – stars: AGB, post-AGB – stars: evolution – stars: fundamental parameters – planetary nebulae: individual: LoTr 4

1. Introduction

The planetary nebula (PN) LoTr 4 (PN G 291.4+19.2, $\alpha_{1950} = 11^{\rm h}49^{\rm m}57\overset{\rm s}{.}7$, $\delta_{1950} = -42°00'56''$) was discovered by Holmberg et al. (1978) and confirmed to be a PN by Longmore & Tritton (1980).

Its prominent central star (CSPN) is very hot and hydrogen-deficient, exhibiting an almost pure He II absorption-line spectra (Fig. 9). According to the classification scheme of Méndez (1991) it belongs to the O(He) subtype in contrast to related objects which also show strong C IV absorptions (subtype O(C) or PG 1159). It is worthwhile to note that only two objects of the O(He) subtype are known (the other is the CSPN K 1-27) whereas 14 PG 1159-type CSPN are identified which have similar effective temperatures and surface gravities (Fig. 24) but show additionally strong C IV absorptions.

We had recently analyzed the PN K 1-27 (Rauch et al. 1994, henceforth Paper I) and found for its exciting central star $T_{\rm eff} = 100 \pm 15$kK, $\log g = 6.5 \pm 0.3$, $n_{\rm N}/n_{\rm He} = 0.005$ (by number), and upper limits of $n_{\rm N}/n_{\rm He} = 0.005$ and $n_{\rm C}/n_{\rm He} < 0.005$. These photospheric abundances indicate that K 1-27 could be a "born-again post-AGB star" according to the evolutionary scenario of Iben et al. (1983). The same scenario has been proposed to hold for the PG 1159 stars (Werner et al. 1991). It predicts that a star experiences a late He flash at already decreasing luminosity after its first departure from the AGB. The star returns to the AGB and in a second, He-burning post-AGB phase, a stellar wind — as predicted by radiation driven wind theory (Pauldrach et al. 1988) — will take off the H-rich envelope completely and lay free first He-rich and later carbon and oxygen-rich material. Thus, the nebula metallicity, reflecting the photospheric composition at the time of its ejection, should be higher in the inner

Send offprint requests to: T. Rauch
* Based on observations collected at the European Southern Observatory (La Silla, Chile); this research has made use of the Simbad database, operated at CDS, Strasbourg, France

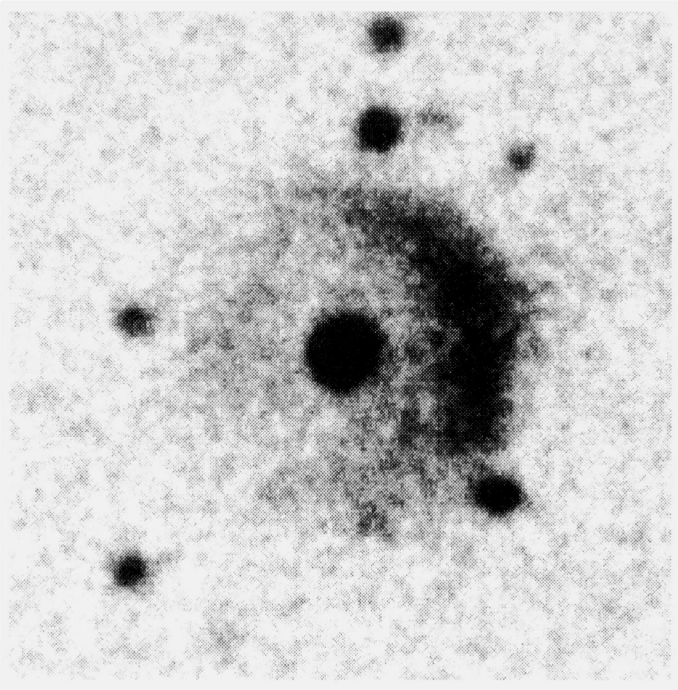

Fig. 1. The PN LoTr 4 in a reproduction from the ESO SRC survey (J 320, orientation: north down, east right). This and all following images are covering a region of 60″ × 60″

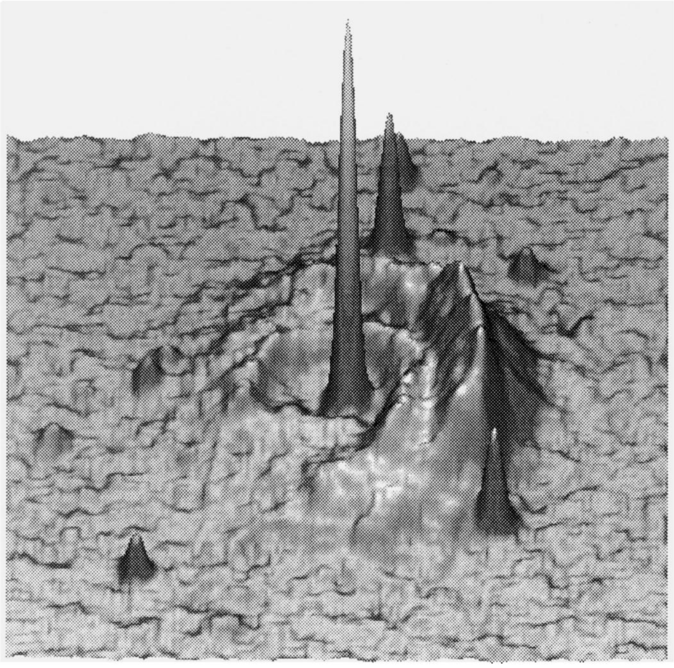

Fig. 2. Distribution of the surface brightness in H α (normalized to the local background) of the PN LoTr 4 (image no. 1), smoothed using a boxcar average of 1″. The intensity scale is linear. The peak height at the central star is 8.6 in arbitrary units

part of the nebula than in the outer part. However, in the case of K 1-27 no abundance gradient was found in the nebula (Paper I).

In this paper we will first have a look onto the structure of LoTr 4, especially on its spatial distribution (Sect. 2.1), and describe our spectroscopic observations of its central star (Sect. 2.2). A detailed analysis of the central star is carried out by means of NLTE model atmosphere techniques (Sect. 3). An analysis of the nebula follows in Sect. 4. At the end we will consider how LoTr 4 fits in our picture of post-AGB evolution (Sect. 5).

Table 1. Observation log of the direct images taken at ESO (La Silla, Chile). The image numbers given are referred to in the text

No.	telescope	instrument	ESO filter	time / min	date
1	2.2m	EFOSC 2	# 694 H α	10	6-Feb-95
2			# 689 [O III]	10	6-Feb-95
3	NTT	EMMI	# 654 H α	20	10-Apr-95
4			# 589 [O III]	20	10-Apr-95
5			# 588 He II	20	10-Apr-95
6			# 654 H α	40	10-Apr-95

2. Observations

2.1. Direct imagery of the nebula

Whereas the finding chart in the catalogue of Acker et al.(1992) shows merely a faint nebulosity, inspection of the ESO-SRC J plate (Fig. 1) and of the images taken by Schwarz et al.(1992) reveals that the nebula consists of a bright arc on the eastern limb, and some fainter emission around the central star.

In order to investigate the spatial structure of the nebula and the distribution of matter in the nebula more closely, we had recently taken direct images (H α and [O III] λ 5007 Å) of LoTr 4 at ESO (Table 1). At the 2.2m telescope we used the CCD ESO # 19 (THX 31156, 19μ, 1024×1024 px, 0.336″ / px). On the H α image two clearly separated shells within the PN became visible. Although the multiple-shell phenomenon is prevalent in PN (Chu 1989) we decided to take deeper images at the 3.5m NTT[1] at ESO with the CCD ESO # 36 (TEK TK 2048 EB, 24μ, 2048×2047 px, 0.268″ / px) because the PN is rather faint (Sect. 3.3) and its structures on the western side nearly disappear in the background continuum. In addition, we took one image with a He II λ 4686Å filter in order to measure directly the He II λ 4686Å / H α intensity ratio. All images were flatfielded with suitable dome flats.

Fig. 2 shows a surface plot of the H α - brightness distribution across the nebula's face. The prominent narrow peaks are due to the central star and background stars. The ridge from the bright eastern segment is clearly visible. It extends in an arc at the outer edge of the nebula, and is clearly discernible in the southern part. As the figure shows, the ridge consists of three peaks. No trace can be found on the northern and western sides. Inside this arc, one finds another structure, forming a ridge of emission of lower surface brightness, and surrounding the central star almost completely. In grayscale representation (Fig. 3)

[1] New Technology Telescope

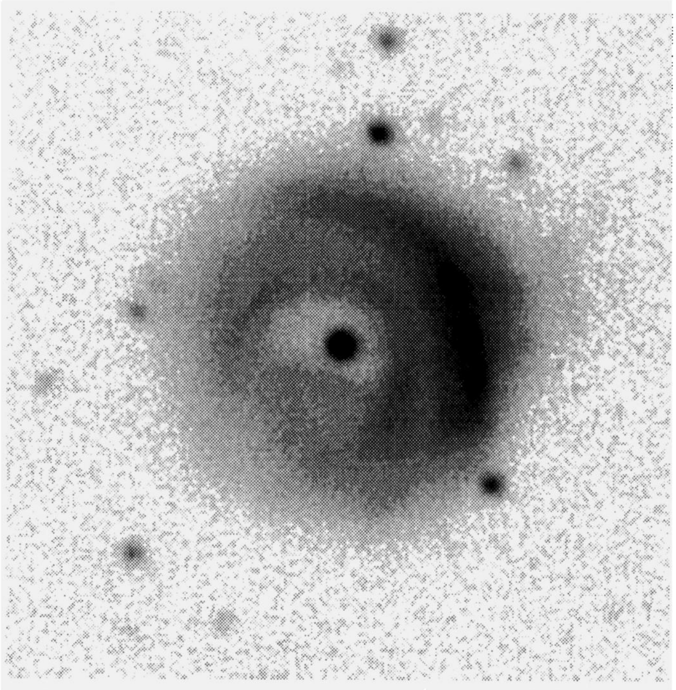

Fig. 3. H α image (image no. 6) of the PN LoTr 4. The visible nebula dimensions are about 37″ in W-E and 39″ in N-S direction. Note that a maximum extension is found in ESE direction (Sect. 2.1.1)

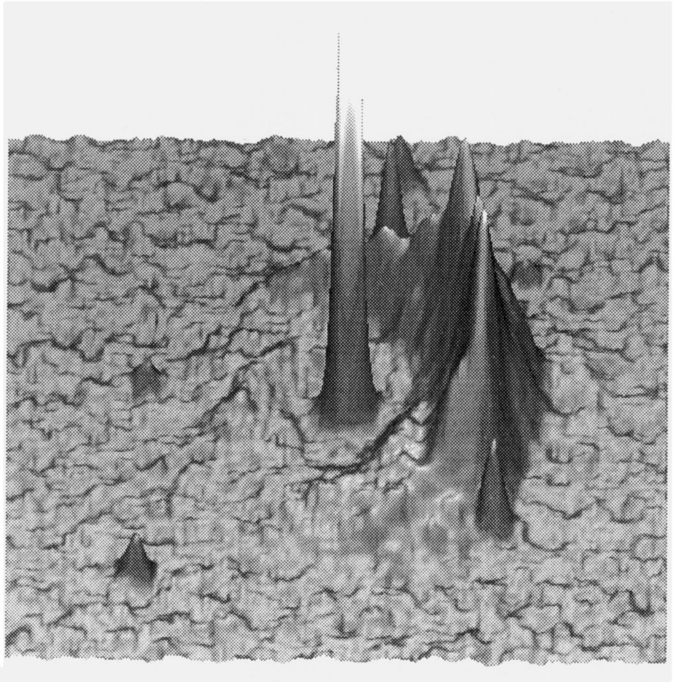

Fig. 4. Same as Fig. 2, from the [O III] λ 5007 Å image (no. 2)

one notes that this inner nebula consists of several filament-like streaks of emission, and that it is not symmetric about the central star, but forms a larger inner hole in the NW quadrant. The largest nebula extension is found towards ESE.

In the [O III] λ 5007 Å image (Fig. 4) the outer eastern segment is very prominent, but the emission covers the same region as that of H α. The inner nebula is also discernible at lower intensity. In this image, we find emission in south-east direction 22.5″ away from the central star which can be a fragment of a third nebula shell (Fig. 5).

2.1.1. Properties of the shells

The [O III] λ 5007 Å / H α intensity ratio (not shown but easily to imagine from Fig. 2 and 4) is very high in the eastern segment. At a position angle of about 80 degrees, one notes a depression in the ridge, and that there the low level emission reaches out to larger radii. One could get the impression that in this direction the stellar photons transverse a more transparent outer shell and enhance the ionization of matter further out. However, since the visible nebula is optically thin to the He II Lyman continuum (Table 4), any matter outside would show up strongly in [O III] from the He^+ zone. Thus, the extension of the emission does not reflect an enhancement of the ionization, but a genuine extension of the nebula.

Quite remarkable is the region of the inner nebula: here the intensity ratio is much lower than in the outer segment, but the ratio is quite constant throughout the region: between 0.7 and 0.9 in our arbitrary units. This is also depicted in Fig. 6 as a W-E slice across the nebula, taken from our ’94 EMMI spectra (note that the arbitrary intensity scales are different). From the H α image one gets the impression that the inner nebula is a shell with a relative thickness of about 30 - 50%. The constancy of the [O III] / H α ratio implies that within the shell the radial variation of the ionic abundance ratio O^{2+} / He^+ should be rather small. Since the O^{2+} density depends on the distance from the central star, and may vary in the He^{2+} zone (Fig. 12, Paper I), this means that the inner nebula consists of a rather thin shell, of not more than about 30% relative thickness.

Fig. 7 shows that the He II / H α ratio varies only little (between 0.6 and 0.7) across the face of the inner nebula, seen in the western part. Being formed by recombination, both lines are quite insensitive to local variations of the electron temperature, so that their ratio directly shows the variation of the abundance ratio. As both hydrogen and helium are fully ionized, the He/H abundance ratio is quite constant in the inner nebula. The line ratio is lower in the bright eastern segment, which is because of the decrease of He^{2+} density in the outer parts of the nebula, due to the ionization stratification (Fig. 12, Paper I).

When we tried a quantitative analysis of the surface brightness distribution of H β with the assumption of spherical shells, it turned out to be impossible to reproduce the profile. Since the emissivity of a recombination line depends only weakly on electron temperature and density, its surface brightness distribution is determined almost exclusively by the distribution of the protons along the lines of sight, i.e. it reflects the spatial distribution of the nebula matter. In Fig. 8 we compare the observed brightness distribution with two models: in the first one, the gas density as a function of distance from the central star is the sum of three Gaussians with parameters adjusted to match

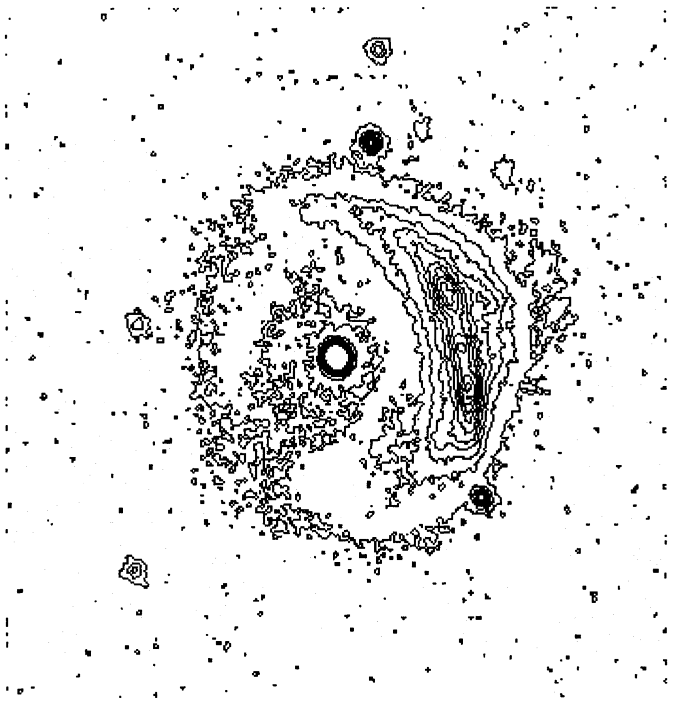

Fig. 5. [O III] λ5007 Å image (no. 4) of LoTr 4 normalized to the background continuum. Note that a 40° emission segment is visible at about 22.5″ from the central star in ESE direction. The isolines start at 1.05 and are spaced by 0.2

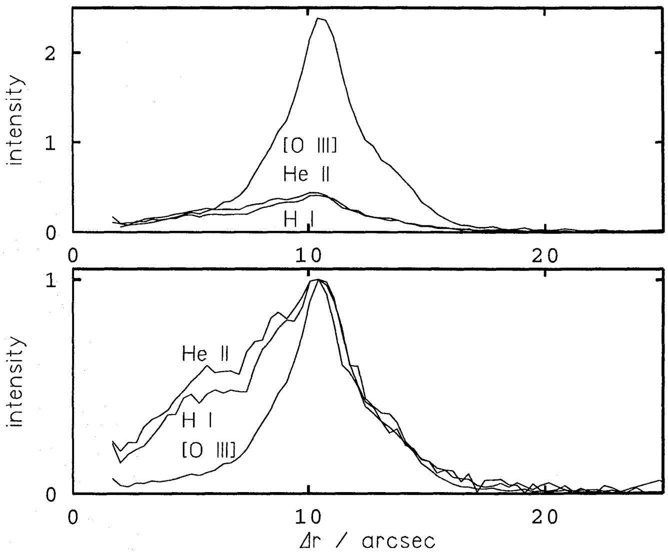

Fig. 6. Intensities (in arbitrary units) of [O III] λ 5007 Å, He II λ 4686Å, and H β in a W-E cut through LoTr 4 (eastern side, compare Fig. 1). The lower picture shows the same intensities normalized to their maximum, respectively

the outer part of the eastern limb. Of course, it gives too high an intensity on the western side. But the intensity in the center of the nebula disk is also too high. In a second one, the parameters were chosen as to match the inner part of the eastern side. Again, one notes that in the region close to the central star the model brightness is too high. To reproduce the large ratio between the maximum and the center with a spherical shell, one would need a relatively thin shell, which implies a narrow profile near the maximum. But this is in conflict with the observed broad maximum. We took this as a strong indication that the nebula not only lacks an W-E symmetry (Fig. 1), but also a symmetry along the line-of-sight. Thus the emission of the eastern side might well arise from a quite narrow segment of a spherical shell.

The outer nebula has an angular radius of 13.5″, and a thickness of about 3″, as estimated from the position and the half-width of the [O III] emission (Fig. 6). The inner shells are between 6 and 9″ from the central star, and have widths of about 3″ or even less.

At the distance of 6 kpc (Sect. 3.3), the inner and outer nebulae have linear radii of 0.22 and 0.39 pc, respectively. Nothing is known about the expansion velocity. Taking a reasonable value of 20 km/sec, one obtains expansion ages of about 10 500 and 19 000 years, respectively.

Since a thin shell of hot (10^4 K) ionized gas would disperse into the surrounding vacuum with the sound speed which is about 10 km/sec, we may roughly estimate the life-time of the structure of the nebula shells. A 3″ thick shell or filament would dissolve in about 10 000 years. As the estimated expansion ages are comparable to this time-scale, it seems most likely that the structures seen may still have retained some of the original features. In particular, if the outer and the inner nebulae were produced in separate events, they would not have had time to fully merge, which is what is observed.

2.1.2. Summary of direct imagery

Because of this, and because the inner nebula seems to be composed of several filaments rather than a perfectly symmetric and homogeneous shell, we tend to believe that the inner nebula could well have been expelled in several ejections in different directions. If its central star is indeed a "born-again post-AGB" star, this means that the expulsion of the nebula after the return to the AGB occurs in a fairly complicated scenario rather than a single event.

The crescent slope of the bright segment is reminiscent of asymmetrical nebulae which have most likely interacted with the ambient medium (cf. Borkowski et al. 1993) which could well have played a rôle in shaping the outer nebula in LoTr 4.

2.2. Spectroscopy of the central star

Two optical spectra of LoTr 4 were obtained in January 1993 (Table 2) with the 3.6m telescope of the ESO at La Silla with EFOSC 1[2] using the blue cross disperser and the CCD ESO#26 (TEK512M 1215-3, 27μ, 512×512 px). The wavelength range covered is about 3725Å≤λ≤8800Å. A 1″ × 9″ slit in W-E direction was used. The data reduction of the echelle spectra was

[2] ESO Faint Object Spectrograph and Camera

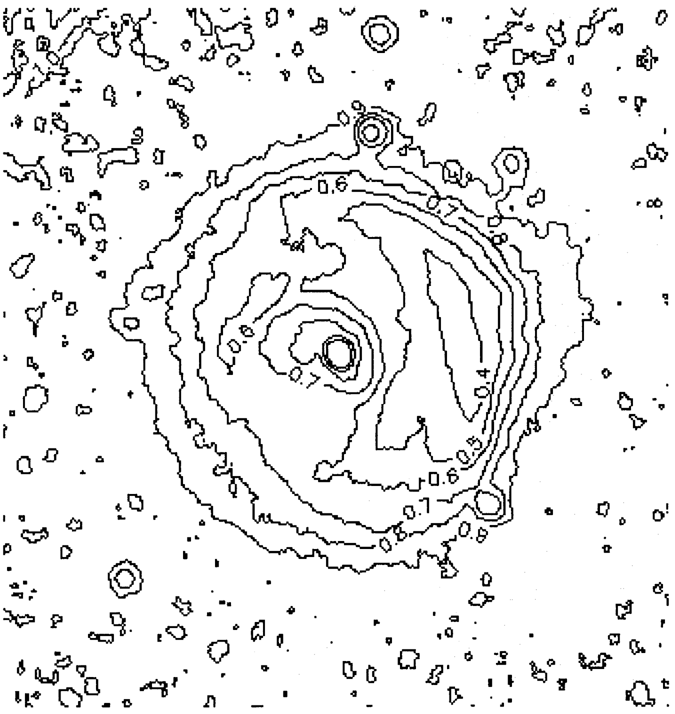

Fig. 7. He II λ 4686Å / H α (image no. 5 / no. 6). The range displayed is 0 to 1, with isolines spaced by 0.1

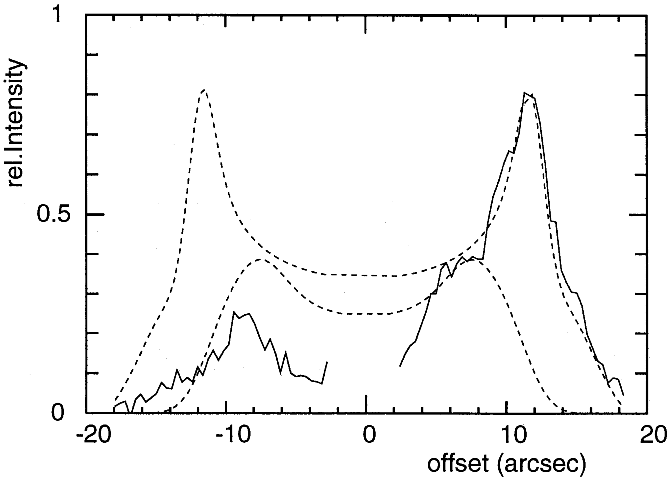

Fig. 8. The variation of the H β surface brightness, observed along the W-E direction (solid), and from two models (dashed) with spherical symmetric, homogeneous shells whose radial density distribution is chosen to match the outer or the inner part of the eastern side

Table 2. Observation log of the analyzed spectra taken at ESO (La Silla, Chile).

telescope	instrument	dispersion Å mm^{-1}	exposure time / min	date	observer
3.6m	EFOSC 1	32-63	40	29-Jan-93	Rauch
3.6m	EFOSC 1	32-63	75	30-Jan-93	Rauch
NTT	EMMI	39	2 × 33	11-Jun-94	Napiwotzki
NTT	EMMI	39	60	8-Apr-95	Rauch
NTT	EMMI	39	60	9-Apr-95	Rauch

carried out using the IRAF[3] software package (Tody 1986). The images were flatfielded with suitable dome flats and wavelength calibrated with He-Ar comparison spectra. A background subtraction was carried out in order to eliminate nebula emissions. The spectra were co-added in order to increase the signal-to-noise ratio. Finally, this observation was smoothed with a Savitzky-Golay filter (Press et al. 1992). We achieve a spectral resolution of $\lambda/\Delta\lambda \approx 1750$.

A first inspection of this spectrum (Fig. 9) immediately shows that there must be a significant contribution of hydrogen, e.g. the He II λ 6560Å / H α blend has its maximum depression at the H α wavelength. In order to ensure that this is not an artifact of our background (and nebula) subtraction (in the EFOSC 1 echelle spectra there are only 1-3 pixels beside the stellar spectra which are useful for this purpose) we decided to take additional long-slit spectra which permit a more precise background subtraction (Fig. 9). Two spectra were taken in June 1994 (Table 2) with the NTT with EMMI[4] in the blue medium dispersion (BLMD) mode (4250Å≤λ≤5100Å). We employed the CCD ESO#31 (TK 1024 AB, 24μ, 1024×1024 px) together with the grid #12 (38Å/mm). The slit (also in W-E direction) width and length projected on the sky were 1.″5 and 178″, respectively. The data reduction of this spectrum had been done using the MIDAS[5] software package (Warmels 1991). These spectra were also co-added in order to increase the signal-to-noise ratio. Two more spectra were taken in April 1995 (Table 2) with the same telescope and instrument (remote observing) in order to measure the wavelength ranges around O VI $\lambda\lambda$ 3811, 3834Å, [Ne III] $\lambda\lambda$3869, 3967Å, and [Ne V] λ3426 Å. The wavelength ranges covered were 3350Å≤λ≤4200Å and 3500Å≤λ≤4300Å. Compared to our '94 EMMI spectra the latter are of much worse quality most probably due to weather conditions.

In Fig. 9 we compare the optical spectra of the central stars of LoTr 4 and K 1-27 which appear rather similar: the He II absorption lines $\lambda\lambda$4686, 6560, 5411, 4859, 4541, 4338Å (transitions 3-4, 4-6, ..., 4-10) are conspicuous in both spectra as well as the N V emission lines at 4603/4619Å and 4944Å. The interstellar Na D doublet at $\lambda\lambda$5890, 5896Å is present in both spectra. In the spectrum of LoTr 4 we find additionally He II $\lambda\lambda$ 4100, 4199Å (transitions 4-12, 4-11) and the interstellar Ca II H and K lines at $\lambda\lambda$3969, 3934Å. In the spectrum of K 1-27 we find telluric absorptions, e.g. at $\approx \lambda$6300Å.

3 IRAF is distributed by the National Optical Astronomy Observatories, which is operated by the Association of Universities for Research in Astronomy, Inc. (AURA) under cooperative agreement with the National Science Foundation

4 ESO Multi Mode Instrument

5 Munich Image Data Analysis System

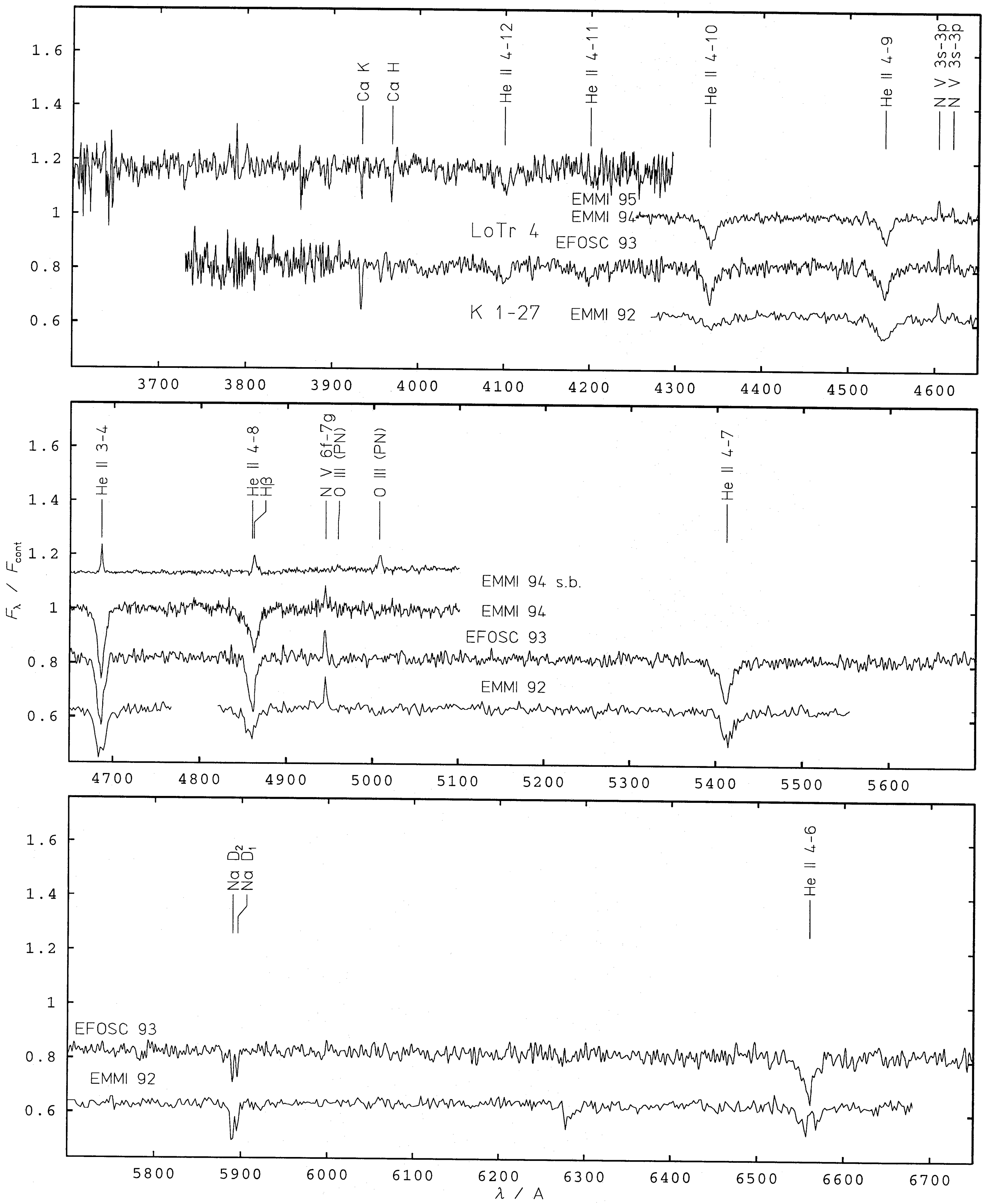

Fig. 9. Normalized spectra of the CSPN LoTr 4 and K 1-27 (at the bottom in all figures). Their resolution ($\lambda/\Delta\lambda$) is about 1750 (LoTr 4, for both EMMI and EFOSC 1) and 1450, respectively. The identified lines are marked. In case of the LoTr 4 EMMI 94 spectrum the subtracted background (s.b.) is additionally shown which allows to judge the quality of the data reduction

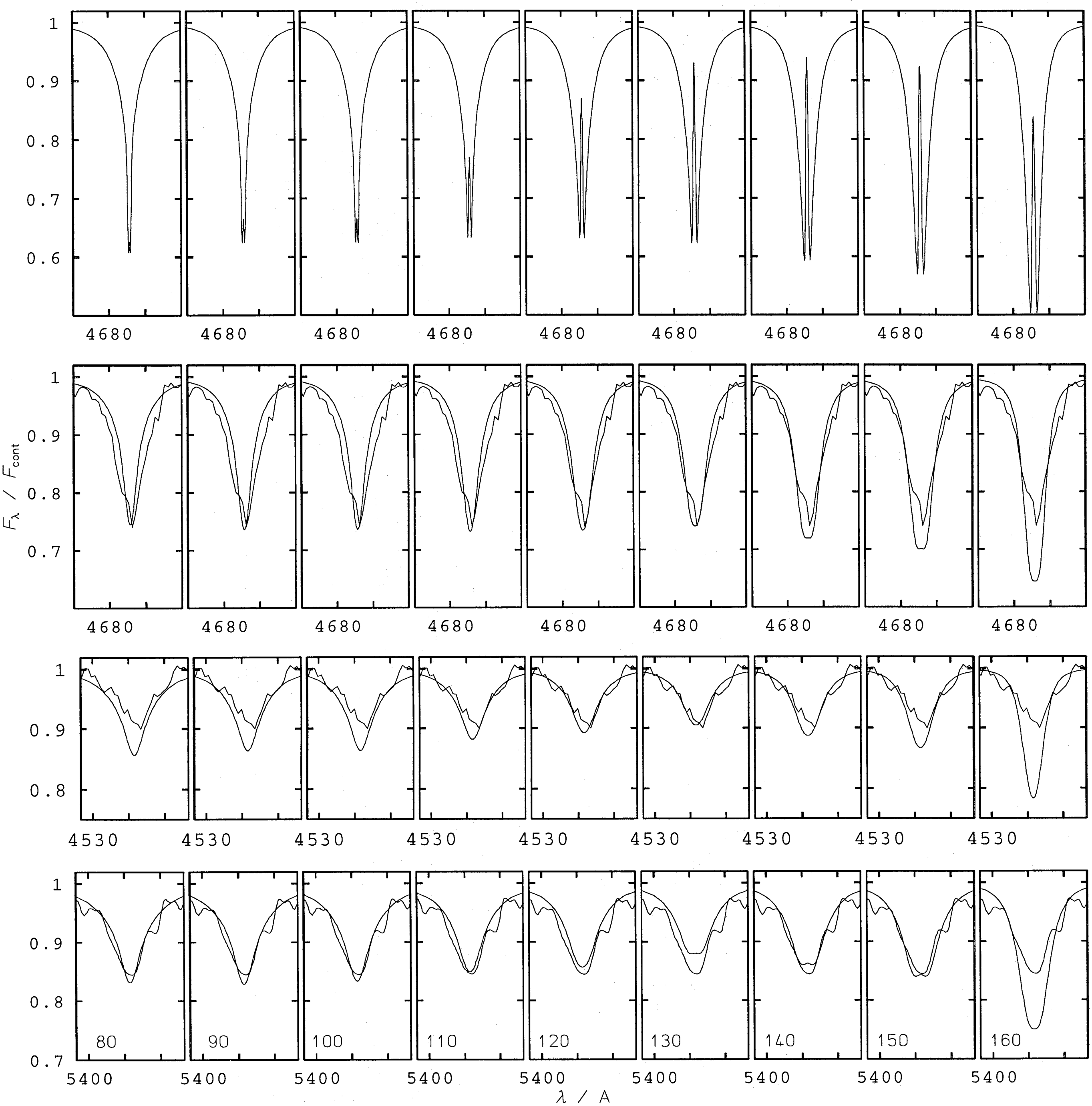

Fig. 10. Dependency of He II line profiles on $T_{\rm eff}$. Theoretical line profiles of He II λ4686Å (3 – 4, top rows) and He II $\lambda\lambda$4541, 5411Å (4 – 9, 4 – 7) are shown for $T_{\rm eff}=80-160$kK, $\log g=5.5$, and $n_{\rm H}/n_{\rm He}=0.01$. The profiles of rows 2, 3, and 4 are convoluted with a Gaussian (FWHM= $\lambda_\circ/1750$, see Sect. 2) in order to compare them to the spectrum of LoTr 4 (Sect. 3.1)

3. NLTE analysis of the central star

For the analysis of the central star of LoTr 4 we used a grid of plane-parallel, hydrostatic NLTE model atmospheres (see Paper I). The models were calculated with the same model atoms using our Accelerated Lambda Iteration (ALI) code (Werner 1986). An improvement has been made by including the Hummer-Mihalas (1988) occupation probability formalism for H I and He II (Werner 1995).

For the comparison with observations in the wavelength range Hγ – Hβ we will use the EMMI 94 spectrum (due to the better background subtraction) and outside this range the EFOSC 1 and EMMI 95 spectra.

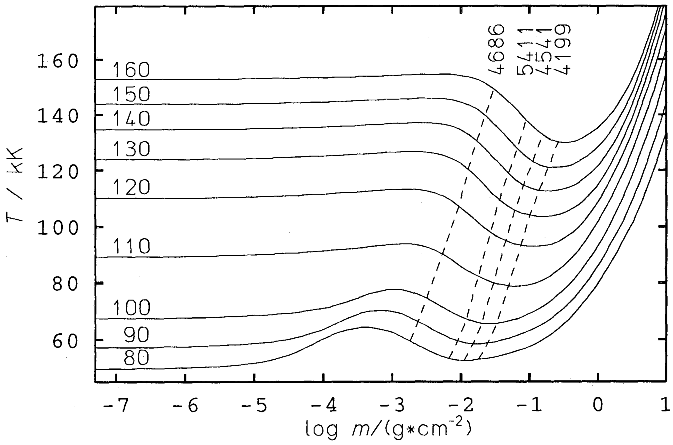

Fig. 11. Temperature stratification of our H-He model atmospheres with $\log g = 5.5$, $n_{\rm H}/n_{\rm He} = 0.01$, and $T_{\rm eff} = 80 - 160$kK. The formation depths ($\tau = 1$) of the line cores of He II λλ 4686, 5411, 4541, 4199Å are marked (dotted lines)

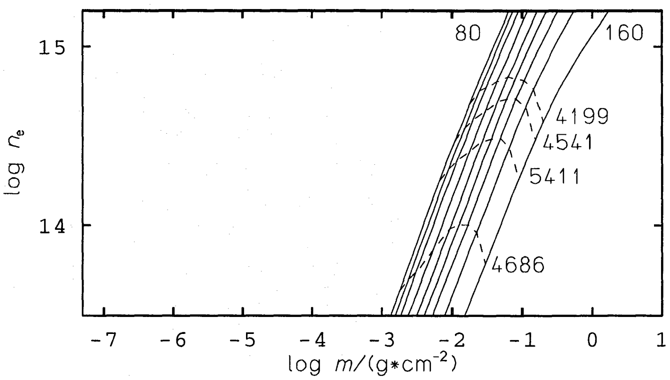

Fig. 12. Electron density in the line forming region as extracted from the models of Fig. 11

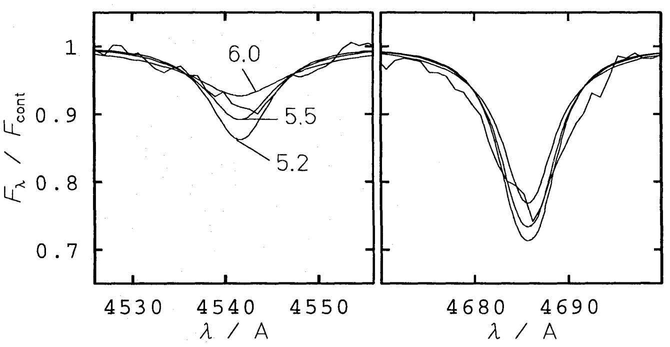

Fig. 13. Theoretical line profiles of He II λλ 4541, 4686Å calculated from model atmospheres with $T_{\rm eff} = 120$kK and $\log g = 5.2, 5.5, 6.0$. Changes at $T_{\rm eff} = 100 - 140$kK are similar

Some test calculations with different H/He ratios within the relevant $T_{\rm eff} - g$ range show that the He II line profiles are almost saturated for $n_{\rm H}/n_{\rm He} < 0.2$ and at $T_{\rm eff} = 120$kK and $\log g = 5.5$ they fit best the observations with $n_{\rm H}/n_{\rm He} \approx 0.5$. Thus, we can use already calculated $n_{\rm H}/n_{\rm He} = 0.01$ models for a preliminary analysis of $T_{\rm eff}$ and g (Sect. 3.1). A detailed analysis of the H/He ratio is presented in Sect. 3.2.1.

3.1. Effective temperature and surface gravity

A first series of He II line profiles was calculated from models with $n_{\rm H}/n_{\rm He} = 0.01$, $\log g = 5.5$, and $80{\rm kK} \le T_{\rm eff} \le 160$kK. $T_{\rm eff} \lesssim 70$kK can be excluded from the outset because no He I lines (e.g. He I λ 4471Å, Fig. 9) are observed. The He II line profiles have a minimum depression at $T_{\rm eff} \approx 120$kK and become deeper and broader towards higher $T_{\rm eff}$.

The broader line profiles at higher $T_{\rm eff}$ can be explained by looking at their formation depths (Fig. 11) which lie deeper inside the atmosphere, i.e. at higher temperatures (thermal Doppler broadening, line core) and densities (Stark broadening, wings).

The deeper line cores at higher $T_{\rm eff}$, i.e. at constant g and elemental composition closer to the Eddington limit, are the result of the decreasing density (helium is highly ionized at these temperatures and therefore in good approximation the electron density $n_{\rm e}$ can be taken as a measure of He II in the atmosphere: $n_{\rm He\,II} \sim n_{\rm e}^{-1}$) in the line forming regions (Fig. 12). For all He II lines we found there a density maximum at $T_{\rm eff} \approx 135$kK which is fairly in agreement with Fig. 10.

If we want to compare our theoretical line profiles with the observed spectrum we have to account for the instrumental profile and convolute them with a Gaussian of a respective FWHM (Sect. 2). Due to the formation of He II λ 4686Å (3 − 4, Fowler series) highly in the atmosphere (Fig. 11) where Stark line broadening is less effective the convolved profile becomes monotonously deeper with increasing $T_{\rm eff}$ while line profiles of the Pickering series (4 − n) which form deeper in the atmosphere have a minimum core depth at $T_{\rm eff} \approx 120$kK (Fig. 10).

From this first series of models ($n_{\rm H}/n_{\rm He} = 0.01$, $\log g = 5.5$), the theoretical He II line profiles are equally well matching the observation at $T_{\rm eff} = 120$kK. A $T_{\rm eff}$ lower than 110kK can be excluded from the much deeper He II λ 4541Å while at $T_{\rm eff}$ higher than 130kK He II λ 4686Å is incompatible with the observation. However, for a more tight determination of $T_{\rm eff}$ high resolution ($\lambda/\Delta\lambda \gtrsim 10000$) spectroscopy is necessary in order to measure reliably the emission reversal in He II λ 4686Å which is a sensitive indicator for $T_{\rm eff}$ (Fig. 10).

We investigate the sensitivity of the line profiles on g (Fig. 13): all line profiles change evidently the depth of their line cores while the wings remain nearly unchanged when we vary g: lower values give much deeper line cores and are therefore incompatible with the spectrum. Compared to the dependency on $T_{\rm eff}$ (Fig. 10) a change of $\log g$ by 0.3 is approximately equivalent to a change of $T_{\rm eff}$ by 20kK.

Thus, we can preliminary restrict the parameter range to $T_{\rm eff} = 120 \pm 15$kK and $\log g = 5.5 \pm 0.3$ and analyze now the possible H/He ratio within this range. In order to judge dependencies of abundance ratios on $T_{\rm eff}$, we use in the following two models with $T_{\rm eff} = 110, 130$kK, and $\log g = 5.5$ (which equally well fit the He II lines).

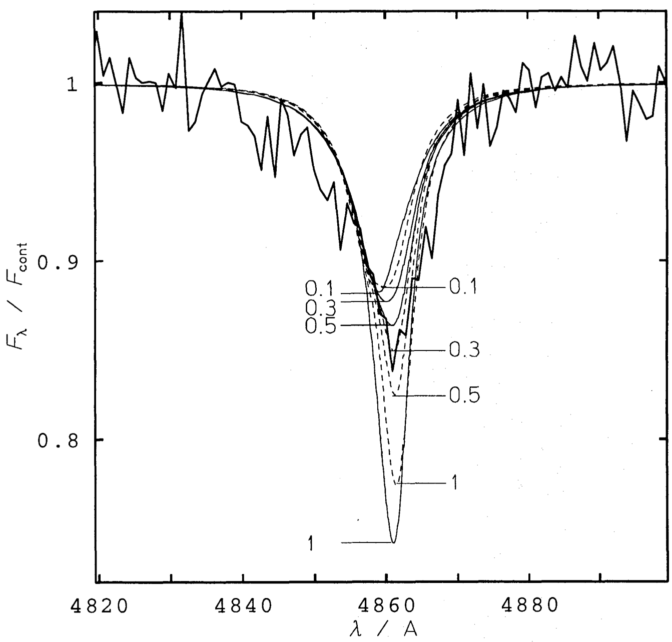

Fig. 14. The He II λ 4859Å / Hβ blend calculated from model atmospheres with $T_{\rm eff}$ = 110kK (fully drawn) and $T_{\rm eff}$ = 130kK (dashed), log g = 5.5, and $n_{\rm H}/n_{\rm He}$ = 1, 0.5, 0.3, 0.1

3.2. *Photospheric abundance ratios*

In the following sections we describe a detailed analysis of the photospheric abundance ratios.

The content of hydrogen in the photospheres of LoTr 4 and K 1-27 is one of the key questions to their evolutionary status. In case of K 1-27 (Paper I), we could only give an upper limit: $n_{\rm H}/n_{\rm He} < 0.2$. In the spectrum of LoTr 4 asymmetries in the blends of He II and H I lines are clearly visible (Fig. 14, 15) and we can determine the H/He ratio.

In analogy to the analysis of K 1-27 we determine the N/He abundance from the N V λ 4944Å complex.

Finally, we give upper limits for the C/He and O/He abundance ratios.

3.2.1. H/He

We calculated H-He model atmospheres with $T_{\rm eff}$ = 110, 130kK, log g = 5.5, and different H/He ratios. In Fig. 14 we show the He II λ 4859Å / Hβ blend compared to the spectrum. At $n_{\rm H}/n_{\rm He}$ = 0.5 we achieve a good agreement at both $T_{\rm eff}$, whereas $n_{\rm H}/n_{\rm He}$ = 1 is definitely too high.

This hydrogen abundance is confirmed by a look on other He II / H I blends (Fig. 15) in the spectra and finally we adopt $n_{\rm H}/n_{\rm He}$ = $0.5^{+0.2}_{-0.3}$.

3.2.2. N/He

In the spectra of LoTr 4 the N V lines 4603/4619Å and 4944Å appear in emission (Fig. 9). We calculated model atmospheres with nitrogen in addition. Within the relevant parameter range

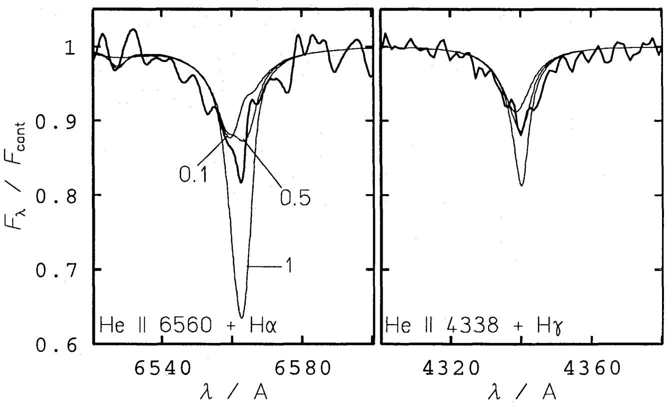

Fig. 15. He II and H I line profiles calculated from model atmospheres with $T_{\rm eff}$ = 120kK, log g = 5.5, and $n_{\rm H}/n_{\rm He}$ = 1, 0.5, 0.1

Table 3. Equivalent widths (emission) of the theoretical N V lines calculated from models with $n_{\rm H}/n_{\rm He}$ = 0.5 and $n_{\rm N}/n_{\rm He}$ = 0.001. The values for the different $n_{\rm N}/n_{\rm He}$ are calculated with log g = 5.5

	N V λλ 4603, 4619Å			N V λ 4944Å		
	log g					
$T_{\rm eff}$ / kK	5.2	5.5	5.8	5.2	5.5	5.8
110	343	303	260	205	67	0
120	446	396	353	307	169	93
130	511	461	426	399	209	141
	$n_{\rm N}/n_{\rm He}$ / 10^{-4}					
	5	10	20	5	10	20
120	291	371	396	86	124	169

($T_{\rm eff}$ = 120 ± 15kK, log g = 5.5 ± 0.3) we find the theoretical line profiles always in emission (Fig. 16, 17). Their dependence on variations of $T_{\rm eff}$ and g is summarized in Table 3.

In Paper I we had problems to fit N V λλ 4603, 4619Å and N V λ 4944Å consistently to the spectrum of K 1-27 because the theoretical line profiles of N V λλ 4603, 4619Å are in absorption at the relevant $T_{\rm eff}$ and g (Sect. 1) determined from the He II lines. The reason is still unclear. Thus, in the case of LoTr 4 we start to determine the N/He abundance ratio from N V λ 4944Å. In Fig. 16 we compare theoretical line profiles to the spectrum of LoTr 4. They appear in emission at lower ratios and change to absorption towards higher abundances. At $n_{\rm N}/n_{\rm He}$ = 0.001 (solar ratio) we achieve a good fit to the observed profile whereas at both, lower and higher abundances the theoretical line profiles do not reach the peak height of the observed emission.

A nitrogen abundance of $0.0005 \lesssim n_{\rm N}/n_{\rm He} \lesssim 0.001$ also fits N V λλ 4603, 4619Å (Fig. 17).

For the calculation of the N V line profiles we used an approximate formula (Werner et al. 1991, Paper I). For the N V λ 4944Å complex new line broadening tables are available (Schöning 1995). We calculated a profile from our model with $T_{\rm eff}$ = 120kK, log g = 5.5, $n_{\rm H}/n_{\rm He}$ = 0.5, and $n_{\rm N}/n_{\rm He}$ = 0.001 and compared it to our "approximate" profiles: the shape is similar with a 30% smaller equivalent width. Regarding the dependence

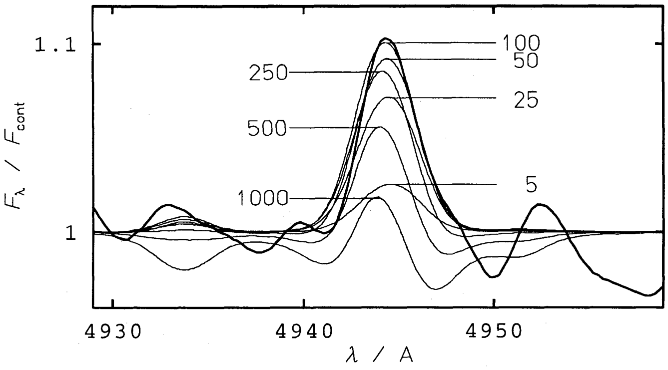

Fig. 16. The N v $\lambda\,4944$Å complex calculated from model atmospheres ($n_{\rm He}/n_{\rm H}=2$) with $T_{\rm eff}=120$kK, $\log g=5.5$ and $n_{\rm N}/n_{\rm He}$ = 5, …, $1000 \cdot 10^{-5}$. The calculated profile matches the observation at $n_{\rm N}/n_{\rm He}=0.001$. Note the wavelength shift (≈ -1.3Å) of the emission maximum for $n_{\rm N}/n_{\rm He} \gtrsim 0.001$ due to the different strengths of the blended components (N v 6-7, cf. Moore 1971) which contradicts these abundances

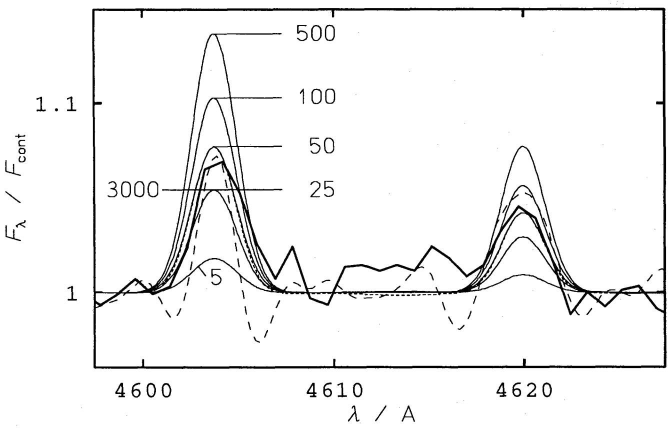

Fig. 17. The N v $\lambda\lambda\,4603, 4619$Å doublet calculated from model atmospheres with $T_{\rm eff}=120$kK, $\log g=5.5$, $n_{\rm H}/n_{\rm He}=0.5$, and $n_{\rm N}/n_{\rm He}$ = 5, …, $3000 \cdot 10^{-5}$. A maximum of the emission is found at $n_{\rm N}/n_{\rm He}=0.005$. The observations (EFOSC 93: – – – and EMMI 94 ——) are reproduced at $0.0005 \lesssim n_{\rm N}/n_{\rm He} \lesssim 0.001$

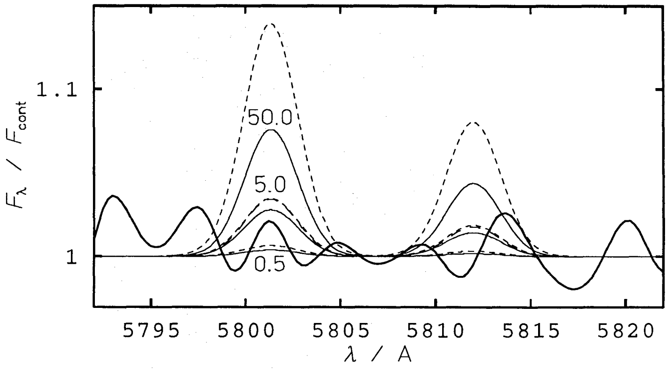

Fig. 18. The C iv $\lambda\lambda\,5801, 5812$Å doublet calculated from model atmospheres with $T_{\rm eff}=110$kK (fully drawn) and $T_{\rm eff}=130$kK (dashed), $\log g=5.5$, $n_{\rm H}/n_{\rm He}=0.5$, and $n_{\rm C}/n_{\rm He}$ = 0.5, 5.0, $50.0 \cdot 10^{-4}$. An additional profile with $T_{\rm eff}=110$kK, $\log g=5.8$, and $n_{\rm C}/n_{\rm He}=50.0 \cdot 10^{-4}$ is almost hidden by the profile $T_{\rm eff}=130$kK, $n_{\rm C}/n_{\rm He}=5.0 \cdot 10^{-4}$

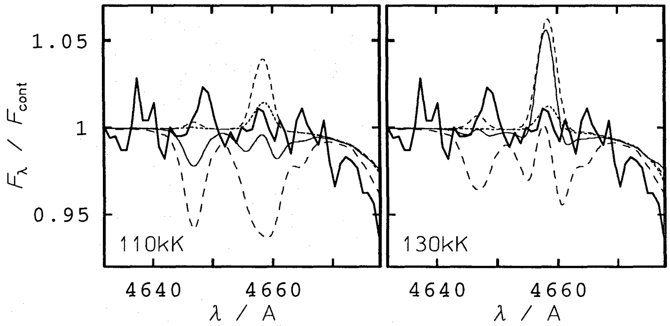

Fig. 19. The C iv $\lambda\,4658$Å complex calculated from model atmospheres with $T_{\rm eff}=110, 130$kK, $\log g=5.5$, $n_{\rm H}/n_{\rm He}=0.5$, and $n_{\rm C}/n_{\rm He}$ = $5 \cdot 10^{-5}$ (- - -), $5 \cdot 10^{-4}$ (– – –), $5 \cdot 10^{-3}$ (—, solar ratio), and $2 \cdot 10^{-2}$ (— — —). Note that the C lines appear firstly at $n_{\rm C}/n_{\rm He}=5 \cdot 10^{-5}$ in emission. The emission increases with the C/He ratio until the line wings develop and the feature changes completely into absorption. At $n_{\rm C}/n_{\rm He}$ ratios higher than solar, the profile is incompatible with the observation

of the theoretical line profile on $T_{\rm eff}$ and $\log g$ (Table 3) we find it in agreement with our calculations. Thus, we determine a solar N/He ratio (0.001) in the photosphere of LoTr 4.

3.2.3. C/He

In our spectra of LoTr 4 no carbon line is detected. Therefore we can only determine an upper abundance limit. The C iv $\lambda\lambda\,5801, 5812$Å (3s-3p) doublet is a sensitive indicator (Fig. 18). We find it always in emission within our parameter range. At $\log g=5.5$ and $n_{\rm C}/n_{\rm He} \gtrsim 0.0005$ (≈ 0.1 solar) the theoretical line profile is incompatible with the observation (Fig. 18). The same value is derived from the C iv $\lambda\,4441$Å (5p-6d) absorption line (not shown). At $\log g=5.8$, $n_{\rm C}/n_{\rm He}=0.005$ (solar ratio) is the upper limit. This limit can be determined also from the C iv $\lambda\,4658$Å complex (Fig. 19). At $n_{\rm C}/n_{\rm He}=5 \cdot 10^{-5}$ emission reversals become visible which are not found in the observations. At $n_{\rm C}/n_{\rm He}=5 \cdot 10^{-3}$ the emission feature changes to absorption due to the formation of strong line wings. Thus, we adopt the solar ratio $n_{\rm C}/n_{\rm He}=0.004$ as an upper limit.

3.2.4. O/He

In order to determine an upper limit for the O/He ratio, we calculated profiles of the O vi $\lambda\lambda\,5274\ldots5290$Å ($n$ = 7 $\leftrightarrow$ 8) complex (cf. Moore 1980). As could be expected, it shows the same behavior like the C iv $\lambda\,4658$Å (n = 5 $\leftrightarrow$ 6) complex (Fig. 19): at lower ratios ($n_{\rm O}/n_{\rm He} \lesssim 0.0005$) it appears mainly in emission and changes into absorption with increasing abundance (Fig. 20).

Another line, O vi $\lambda\,5581$Å ($7{\rm p}\,^2{\rm P^o} - 8{\rm s}\,^2{\rm S}$), confirms an upper limit of about $n_{\rm O}/n_{\rm He}=0.005$. Even more sensitive appear O vi $\lambda\lambda\,3811, 3834$Å ($3{\rm s}\,^2{\rm S} - 3{\rm p}\,^2{\rm P^o}$), which are also incompatible with the observation at this abundance (Fig. 21).

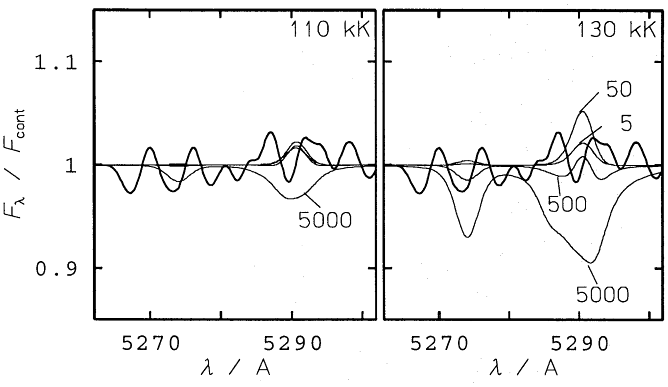

Fig. 20. The O VI λ 5274Å complex calculated from our model atmospheres with $T_{eff}=110, 130$kK, $\log g=5.5$, $n_H/n_{He}=0.5$, and n_O/n_{He} = 5, 50, 500, and 5000 $\cdot 10^{-5}$

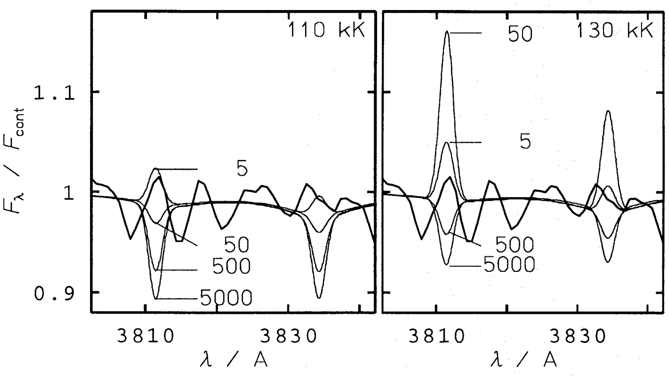

Fig. 21. Same as Fig. 20 for O VI $\lambda\lambda$ 3811, 3834Å. For the calculation of the line profile we used the broadening tables of Dimitrijević & Sahal-Bréchot (1992). Note that the He II $\lambda\lambda$ 3813, 3833Å (4-19, 4-18) and H I λ 3836Å (2-9) lines are responsible for visible the broad depressions around both O VI lines

Thus, we adopt the solar O/He ratio (0.008) as an upper limit for the oxygen abundance. It is worthwhile to note that even the strongest O V lines in the optical wavelength range, O V λ 5114Å ($3s\,^1S - 3p\,^1P^o$) and O V $\lambda\lambda$ 5571 ... 5604Å ($3p\,^3P^o - 3d\,^3D$) are too weak to detect them at this abundance in our spectra.

3.3. Mass and distance

In Fig. 24 we compare the position of LoTr 4 to standard evolutionary tracks in the $\log g - \log T_{eff}$ diagram. We derive a stellar mass of $M/M_\odot = 0.65^{+0.11}_{-0.08}$ with a stellar radius of $R_*/R_\odot = 0.16 - 0.36$ (within $5.2 \lesssim \log g \lesssim 5.8$).

The brightness of LoTr 4 has been measured by Fredrick & West ($m_B = 16.1$, 1984) and Napiwotzki ($m_V = 16.5$, priv. com.). Both values are in good agreement (e.g. Allen 1973). The value of m_V is corrected ($m_{V_0} = m_V - 2.175c$) for the extinction ($c = 0.37$) which is measured from the nebula Hα/Hβ ratio (Sect. 4.1).

Analogously to Paper I we determine the distance using the flux calibration of Heber et al. (1984). From our final model ($T_{eff}=120$kK, $\log g=5.5$, $n_H/n_{He}=0.5$, $n_N/n_{He}=0.001$) we derive an Eddington flux of $H_\nu = 1.88 \cdot 10^{-3}$erg cm^{-2} sec^{-1} Hz^{-1} (at λ = 5454Å). We calculate

$$d = 7.11 \cdot 10^4 \sqrt{H_\nu \cdot M \cdot 10^{0.4 m_{V_0} - \log g}}\ \text{pc} \tag{1}$$

and derive $d = 6.0^{+2.2}_{-2.8}$ kpc. Note that the main error (about $\frac{3}{4}$ of the total) is due to the error in g. The height above the galactic plane is $z = 2.0^{+0.7}_{-0.9}$ kpc, the radius of the nebula is $R = 0.6^{+0.2}_{-0.3}$ pc.

3.3.1. Summary of the analysis of the central star

In summary, we find the following parameters:

T_{eff}	=	120	±15kK
$\log g$	=	5.5	±0.3
n_H/n_{He}	=	0.5	$^{+0.2}_{-0.3}$
n_C/n_{He}	<	0.004	
n_N/n_{He}	=	0.001	±0.5 dex
n_O/n_{He}	<	0.008	
$M_*/M_\odot$	=	0.65	$^{+0.11}_{-0.08}$
$R_*/R_\odot$	=	0.24	$^{+0.12}_{-0.08}$
$\log L_*/L_\odot$	=	4.0	±0.5
d / kpc	=	6.0	$^{+2.2}_{-2.8}$

4. Analysis of the nebula

4.1. Observational data

The spectrum taken by B. Stenholm with the IDS[6] at the ESO 1.2m telescope on Jan. 23, 1986 (Acker et al. 1992) shows the typical features of a high-excitation, strongly density bounded object: The intensity ratio He II λ 4686Å / Hβ is close to 1.1, the value for emission from a nebula consisting of the He^{2+} Strömgren sphere only (with solar He/H abundance ratio). The weakness of [O III] λ 5007 Å and the complete absence of low ionic species, including He I, confirms that the nebula must be optically thin in the H I Lyman continuum. Thus this object resembles rather closely the nebula K 1-27 which had previously been analyzed (Paper I).

The IDS spectrum yields the intensity ratio Hα/Hβ of 3.76 from which an extinction parameter c = 0.37 is obtained with the assumption of T_e = 10kK. However, the intensity ratio of [O III] 5007 and 4959 Å of 2.0 is in strong disagreement with the theoretical value of 2.88, indicating a rather insufficient quality of that spectrum. Therefore, we extracted from our EMMI spectrum nebula emission lines in the wavelength range from 4300 to 5000 Å, integrating over the whole section of the nebula covered by the spectrograph's slit. We obtain a much more satisfactory [O III] intensity ratio of 2.9. The [O III] lines are about 30% stronger than in the IDS spectrum, but as our spectrum also permits the measurement of the weak [O III] 4363 line, we prefer to use our line fluxes. The measured line intensities, corrected

[6] Image Dissector Scanner

Table 4. Intensities $I(\lambda)$ of the nebula lines (normalized to $I(\mathrm{H}\,\beta)$ = 100), as observed and from models with flux distributions with different values of T_{eff}, given in kK

		$I(\lambda)$			
λ/Å	ident.	obs.	110	120	130
F(H β)/(10^{-15} W/m^2)			1.51	1.49	1.52
1034	[O VI]	–	12	108	300
1216	[O V]	–	42	212	351
1240	N V	–	40	128	157
1401	[O IV]	–	64	156	192
1485	[N IV]	–	37	51	42
1550	C IV	–	207	387	485
1640	He II	–	752	760	768
1666	[O III]	–	19	24	26
2423	[Ne IV]	–	187	298	284
2782	[Mg V]	–	20	63	75
3426	[Ne V]	–	85	216	278
3869	[Ne III]	–	61	49	38
3967	[Ne III]	–	19	15	12
4340	H γ	40	47	47	47
4363	[O III]	8.2	5.9	8.2	9.2
4686	He II	110	113	110	110
4711	[Ar IV]	18:	12	6.1	3.5
4740	[Ar IV]	11:	8	4.2	2.5
4861	H β	100	100	100	100
4959	[O III]	120	121	121	121
5007	[O III]	350	348	348	350
5876	He I	–	0.8	0.7	0.6
6563	H α	285	281	278	278
7006	[Ar V]	–	13	8.8	5.8
1.9 μ	H I	–	32	31	30
4.5 μ	[Mg IV]	–	41	38	31
5.6 μ	[Mg V]	–	58	88	111
7.7 μ	[Ne V]	–	16	38	64
10.5 μ	[S IV]	–	32	57	64
14.3 μ	[Ne V]	–	484	797	884
15.5 μ	[Ne III]	–	35	19	13
24.2 μ	[Ne V]	–	526	861	952
25.9 μ	[O IV]	–	2811	2306	1949
51.8 μ	[O III]	–	46	34	31
88.3 μ	[O III]	–	60	44	40
$R_{\mathrm{source}}/\mathrm{R}_\odot$			0.85	0.46	0.32
n / cm^{-3}			70	75	78
$M_{\mathrm{ion}}/\mathrm{M}_\odot$			0.27	0.29	0.31
τ_{911}			0.02	0.06	0.11
τ_{228}			0.12	0.12	0.11

for interstellar extinction, are listed in Table 4. We also include the intensity of H α from Stenholm's spectrum. The error in the intensities are estimated to be ±3% of H β.

In our '94 EMMI spectrum, the nebula [O III] λ 5007 Å emission is clearly detectable up to 55 px (1 px = 0.37″) east and 45 px west of the central star (Figs. 1, 6). From our H α image we measure an angular diameter of about 39″ (Fig. 3) which is somewhat larger than the value given in the Strasbourg-ESO catalogue (Acker et al. 1992), because of the rather slow decline of the intensity.

The brightness profiles show the following characteristic features: H β and He II λ 4686Å have almost identical profiles, but the [O III] λ 5007 Å emission is relatively weaker in the inner part of the nebula disk (Fig. 6).

The measured flux of the H β line $\log F(\mathrm{H}\,\beta) = -12.8 \pm 0.4$ [mW/m^2] (Acker et al. 1991) gives a de-reddened flux of $3.75 \cdot 10^{-16}$ W/m^2.

4.2. The modelling of the nebula

A high excitation nebula has an inner He^{2+} zone whose extent is governed by the number of photons emitted by the central star at energies above 54 eV. These photons ionize also O^{2+} , so there is no [O III] emission from within the He^{2+} zone, but only from the exterior O^{2+} zone. This is the situation in high-density nebulae where the transition He^+/He^{2+} occurs in a layer much thinner than the nebula radius. The size of the He^{2+} region can be computed from the balance of the number of stellar ionizing photons with the total number of recombinations. In contrast, low-density nebulae around low-luminosity CSPN have broader transition zones, and the classical Strömgren sphere arguments do not strictly apply any longer. There is an overlap of the He^{2+} and O^{2+} zones, whose degree is determined by the combination of stellar radius R_* and nebula density n: $R_*^2 n$ (Köppen 1979). This property is used for the interpretation of the spectrum with the aid of photoionization models.

The information available about our nebula is too scarce to fix uniquely all the model parameters. In order to investigate the sensitivity of the fit and to what extent multiple solutions are possible, we give some analytical considerations to how we shall match the observations.

The observational constraints are: the angular diameter a, the H β flux F, and the intensity ratio of the [O III] λ 5007 Å and He II λ 4686Å lines. As unknown parameters we shall consider the distance d, the gas density n in the nebula, the abundances of helium $n(\mathrm{He})/n(\mathrm{H})$ and oxygen $n(\mathrm{O})/n(\mathrm{H})$. Since the stellar models show a deficit of the number of ionizing photons in the He II Lyman continuum, we must also allow for a variation of the flux distribution above 54 eV. This is done by altering all the fluxes above 54 eV by the same factor $(R_{\mathrm{source}}/R_*)^2$, where R_{source} denotes the radius of the ionizing source. To make up the deficit, one has $R_{\mathrm{source}} > R_*$.

From the first constraint one gets a condition for the outer radius R_{outer} of the nebula:

$$R_{\mathrm{outer}} \propto ad \tag{2}$$

To match the H β flux

$$F \propto d^{-2} n^2 \mathrm{Vol} \propto d n^2 a^3 \tag{3}$$

(Vol is the nebula volume) one needs to adjust the gas density in the nebula:

$$n \propto d^{-1/2} F^{1/2} a^{-3/2} \tag{4}$$

The intensity ratio of the [O III] $\lambda\,5007$ Å and He II $\lambda\,4686$Å lines can be estimated as

$$\frac{I(5007)}{I(4686)} \propto \frac{n(\mathrm{O}^{2+})n_e \mathrm{Vol}(\mathrm{O}^{2+})}{n(\mathrm{He}^{2+})n_e \mathrm{Vol}(\mathrm{He}^{2+})} \qquad (5)$$

where we neglect the dependence of the emissivities per ion on electron temperature. The photoionization models show (Fig. 12, Paper I) that both He^{2+} and O^{2+} densities do not vary much in the nebula, we may assume that the volumes in which the ions are dominant have a constant ratio. Note that because we consider the nebula as being optically thin in the He II Lyman continuum, the flux in the He II line is proportional to the helium abundance, unlike the case of a complete Strömgren sphere, where it depends only on the number of ionizing stellar photons. To estimate the ionic fractions, we consider the relevant ionization equilibria at a representative point ($r \approx R_{\rm outer}$) in the nebula. For helium one has

$$n(\mathrm{He}^{2+})n_e\alpha = n(\mathrm{He}^{+})w < \sigma J_* > \qquad (6)$$

with the recombination coefficient α, the geometrical dilution factor $w = \left(R_{\rm source}/2r\right)^2$, and the photoionization integral. Note that any change from the stellar flux distribution above 54 eV is taken into account in the dilution factor. Since neutral helium is not important in the He^{2+} zone, we get

$$n(\mathrm{He}^{2+}) \propto n\frac{n(\mathrm{He})}{n(\mathrm{H})}\frac{gw/n_e}{1+gw/n_e} \qquad (7)$$

with the ratio g of the ionization integral and the recombination coefficient. For oxygen, we consider the ionization balance between O^{2+} and O^{3+} , neglecting the presence of all other stages of ionization $\left(n(\mathrm{O}) \approx n(\mathrm{O}^{2+}) + n(\mathrm{O}^{+3})\right)$:

$$n(\mathrm{O}^{+3})n_e\alpha = n(\mathrm{O}^{2+})w < \sigma J_* > \qquad (8)$$

which gives

$$n(\mathrm{O}^{2+}) \propto n\frac{n(\mathrm{O})}{n(\mathrm{H})}\frac{1}{1+hw/n_e} \qquad (9)$$

with the analogous ratio h which is of the same order of magnitude as g. Thus, one gets

$$\frac{I(5007)}{I(4686)} \propto \frac{n(\mathrm{O})}{n(\mathrm{He})}\frac{1+gw/n_e}{1+hw/n_e}\frac{n_e}{gw} \propto \frac{n(\mathrm{O})}{n(\mathrm{He})}\cdot F^{1/2}a^{1/2}\cdot R_{\rm source}^{-2}d^{3/2} \qquad (10)$$

This simple expression reproduces closely the dependences of the results of the proper photoionization models (see below). It shows that when using the available observational constraints on the nebula, consisting of angular size, total flux, and [O III] / He II line ratio, these data can be matched by various combinations of the parameters, the strongest being the source radius, i.e. the luminosity of the ionizing radiation, followed by the distance. Uncertainties in the Hβ- flux or the angular diameter affect the line ratio only weakly.

The influence on the electron temperature has not been taken into account. But one can qualitatively say that increasing the oxygen abundance or the abundances of all heavy elements increases the cooling rate and thus lowers the temperature in the nebula. Hence, if a model matches the [O III] $\lambda\,5007$ Å intensity, the [O III] $\lambda\,4364$ Å line will come out weaker. In this way, this faint line is an important constraint for the metallicity of the gas.

4.3. Photoionization models

The code GWYN (Köppen 1979) in its interactive version, updated for most recent atomic data, is used to compute the ionization and thermal equilibrium in a spherically symmetric nebula around the central star. The diffuse part of the ionizing radiation is neglected which is a good approximation for nebulae which are optically thin for both hydrogen and helium Lyman continua.

For the ionizing spectrum we use the flux distributions from the model atmospheres with $T_{\rm eff}$= 110, 120, and 130 kK, $\log g$=5.5, $n_{\rm H}/n_{\rm He}$=0.5, $n_{\rm N}/n_{\rm He}$=0.001, and $n_{\rm C}/n_{\rm He}$=0.004. Since the use of the values for the stellar radius obtained earlier (Sect. 3.3) does not lead to a satisfactory fit of the nebula spectrum, we treat the source radius, i.e. the luminosity of the ionizing radiation, as a free parameter.

The nebula is assumed to be a relatively thin spherical shell of constant density, with a ratio of inner and outer radius of $R_{\rm inner}/R_{\rm outer}$ = 0.7 which is suggested from the surface brightness distribution (Fig. 1). Depending on the assumed distance, the outer radius is taken as to give an angular diameter of 37″. The image of the nebula shows that most of the emission comes from the eastern limb, essentially from one quadrant only. As the calculation of the model spectra is done with spherical symmetry, we assume that the flux coming from the whole model nebula is four times larger than observed. The gas density in the shell is assumed to be constant, and is adjusted to match the required total Hβ flux of $1.5\cdot 10^{-15}$ W/m^2. The paucity of the observed nebula lines does not permit us to derive the chemical composition of the gas in detail. We assume that the abundances of the elements heavier than helium follow the pattern in the solar system (from Lang 1980). The common scaling factor $Z/Z_\odot$ shall be a free parameter, as well as the helium abundance.

4.4. Results

In the initial model — distance of 6 kpc, $T_{\rm eff}$ = 120kK, $R_{\rm source}$ = R_* = 0.25R$_\odot$, solar composition, gas densities of around 80 cm^{-3} — the He II line is too weak (by 10%) while the [O III] lines are much too strong (factor 3). In the model with the 110 kK star this discrepancy is much worse, while the 130 kK star gives an acceptable He II line, but the [O III] lines are still twice stronger than observed. One could force a fit by raising the helium abundance and lowering the oxygen content, but it would be rather self-contradictory to have a type I PN with a massive progenitor which is chemically rather old. Evidently the model has too large an optical depth in the He II Lyman continuum, and too large a surrounding O^{2+} zone.

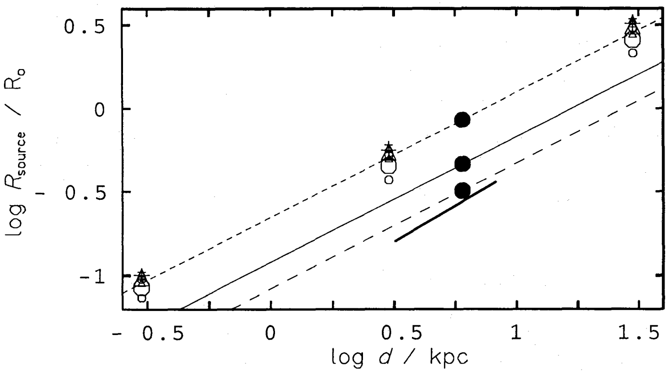

Fig. 22. The loci in the distance – source radius plane for the ionization models that reproduce the angular diameter, the H β-flux, and the He II and [O III] line intensities. The lines connects models with the $T_{\rm eff} = 110$kK star (- - -), 120 kK(—), and 130 kK(– – –). The symbols indicate the metallicity of the nebula ($\log Z/Z_\odot = 0$: △, +0.1 : ○, −0.1 : +). The smaller symbols refer to models with non-solar helium abundances. The thick solid line shows the acceptable range in stellar radius and distance from the stellar photospheric analysis (Sect. 3.3)

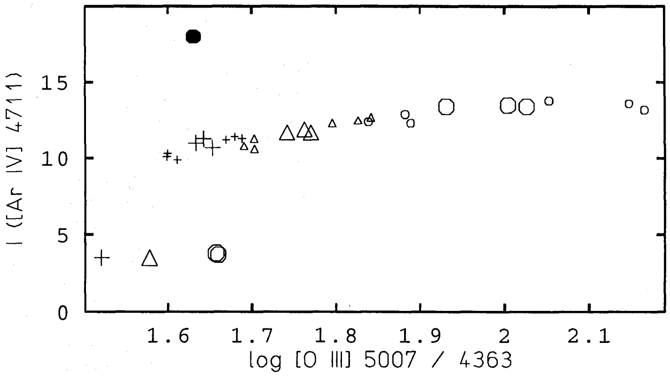

Fig. 23. Comparison of the intensity [Ar IV] λ 4711 Å and the ratio of the [O III] λ 5007 Å / 4363 Å lines, as observed (filled dot) and computed from photoionization models (with the same symbols as in Fig. 22). The upper group of points are $T_{\rm eff} = 110$kK models, the lower 130 kK. Within each metallicity group, the [O III] line ratio increases with increasing distance

Excluding astrophysically unacceptable nebula chemical abundances, Eq. 10 offers two possibilities to explain the observed nebula properties: one could lower the distance of the object, or increase the luminosity of the ionizing source in the He II Lyman continuum. In Fig. 22 we show the loci in the d-$R_{\rm source}$ space of all those models which match the observed angular diameter, H β flux, and the He II λ 4686Å and [O III] λ 5007 Å line intensities. We computed a number of photoionization models with different distances and nebula abundances, adjusting the source radius and nebula density to reproduce the spectrum. For any given ionizing spectrum and nebula chemical composition, all these best fits follow a straight line with the slope 4/3 predicted by our analytical considerations (Eq. 10).

We also constructed models with the helium abundance varied by ±0.1 dex. The loci for models that match the [O III] lines are only slightly altered, so that non-solar helium abundances do not change the quality of the fit. However, none of these models gives an acceptable fit of the helium line. Since the intensity of He II λ 4686Å is proportional to the helium abundance (see above), we can definitely rule out that the helium abundance deviates from 11.00 by more than 0.05 dex (for a 10% error in the observed intensity).

Comparison of the ionization model loci with the $R_{\rm source}$ - d relation obtained from the stellar photospheric analysis shows no intersection. This means that with the stellar radius given from the photometric distance, none of the three stellar flux distributions is able to reproduce the observed nebula spectrum. At least, the model with 130 kK comes closest to that.

If one had only the nebula observations, one could match those data by assuming the same stellar radius but a smaller distance, for instance $R_* = 0.25 R_\odot$ and $T_{\rm eff} = 120$kK would imply $d = 2.5$ kpc. However, this would imply a surface gravity clearly higher than the range permitted from the stellar photospheric analysis. We therefore exclude this possibility.

Thus, the only thing remaining is that the stellar atmospheric models predict too low a flux shortwards of 228 Å. Therefore, we keep the distance of 6 kpc and increase the high energy flux by increasing the radius of the source until the [O III] / He II line ratio is matched with the values given in Table 4. These models are indicated in Fig. 22 as filled circles. One notes two differences in the model spectra: firstly, the electron temperature sensitive ratio [O III] 5007/4363 is well matched by the 120 kK model; in the 110 kK model, the electron temperature is too low, and a better match could easily be effected by lowering the metallicity of the nebula. Conversely, a slight increase in metallicity in the 130 kK model would improve its fit. Secondly, the models differ primarily in the intensities of highly ionized species (e.g. [Ne V], [Mg V]). Measurement of these lines would be very helpful establishing which ionizing spectrum is the best.

The metallicity of the nebula strongly influences the electron temperature, which is measured by the [O III] 5007/4363 line intensity ratio. Fig. 23 shows that this ratio is well reproduced by a metallicity slightly (0.1 dex) below (110 kK star) or above (130 kK) the solar value. This figure also shows that the observed intensity of the [Ar IV] lines appear to be much larger than predicted from any model. However, one must keep in mind that from our spectrum we could only estimate the intensity of this line. Therefore, we do not attach any significance to this "discrepancy" before obtaining better quality spectra, but one notes that the argon lines would pose another constraint on the models.

In a highly density bounded nebula such as LoTr 4, the intensity ratio [O III] / He II depends directly on the local level of ionization (cf. our analytical arguments), so it depends sensitively on the accuracy of the photoionization cross section and the recombination coefficients. While trying to match the nebula spectrum, we also explored whether the failure to match the line intensities could be due to uncertainties in the atomic data. If one wanted to bring the [O III] lines in agreement with observations in the initial 110 kK model by decreasing the ionization $O^{2+} \rightarrow O^{3+}$ or increasing the recombination rate, a factor of about 5 would be necessary. However, such an explanation can not be applied for an explanation of the weakness of the He II line which originates from a hydrogenic configuration. Therefore we think it is rather unlikely that the discrepancy in Fig. 22 is caused by uncertainties in the ionization equilibrium.

While all models match the spectrum quite well, they do not reproduce the distributions of surface brightness observed in H I, He II, and [O III] , shown in Fig. 6 very well, because the density was assumed to be constant in the shell. However, this is not a severe limitation: The prominent features are that the profiles of H I and He II are very similar, while [O III] is more concentrated towards the outer edge of the nebula. As discussed for K 1-27 (Paper I), the former property clearly indicates the absence of any radial variation of the helium abundance within the nebula, the second is the consequence of the ionization stratification.

These characteristic features are also found with the profiles computed from the models, though their exact shape differs from the observed ones. A better match of the shapes can be effected by allowing an appropriate radial variation of the gas density in our spherically symmetric model. But this does not alter the findings we had obtained from matching the spectrum only. Attempts to fit the complete Hβ profile (Fig. 8) with sets of spherically symmetric shells have failed, because the high intensity and the width of the peak and the low brightness in the center of the nebula cannot be satisfactorily matched at the same time. As we had seen in the direct images (Sect. 2.1), [O III] is mainly concentrated in the eastern segment whose true spatial structure is unknown. Because of these strong deviations of the nebula from spherical symmetry, and in view of the still limited observational data of the nebula, we refrain from a fine-tuning of the models to match the surface brightness profiles in detail. But any such fine-tuning will not change our findings on the global nebula properties.

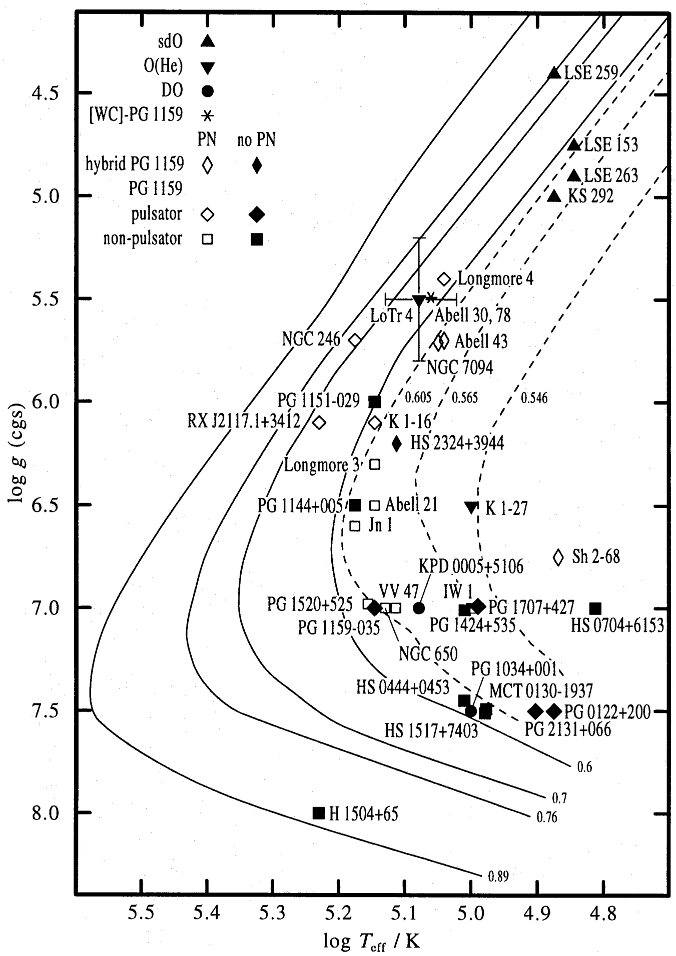

Fig. 24. Position of LoTr 4 in the log g–log $T_{\rm eff}$ diagram compared to theoretical evolutionary tracks of hydrogen burning stars (dashed, Schönberner 1983, Blöcker & Schönberner 1990) and helium burning stars (fully drawn, from Wood & Faulkner 1986, Fig. 1, mass-loss type B). The tracks are labeled with the respective stellar masses (in solar units). Additionally shown are positions of related objects (Dreizler et al. 1995, Rauch & Werner 1995, Werner et al. 1995b, Rauch et al. 1991, Husfeld 1986)

5. Conclusions

From their photospheric parameters, the central stars of LoTr 4 and K 1-27 are found in the same region of the log g – log $T_{\rm eff}$ diagram like the PG 1159 stars (Fig. 24), i.e. they are amongst the hottest stars known. In our present picture an evolutionary sequence [WC]→PG 1159→DO is very likely (see e.g. Werner 1993). Thus we might expect the existence of progenitors of LoTr 4 and K 1-27 exhibiting a Wolf-Rayet type (pure) He II emission line spectrum, however, no such star is known. Also, no cooler central stars with O(He) type spectra as possible progenitor candidates are known. On the other hand, there exist several He-rich post-AGB sdO stars with $T_{\rm eff} \approx$ 70kK resembling a O(He) spectrum (Husfeld et al. 1986, Fig. 24). From its photospheric abundances, KS 292 is very similar to LoTr 4: Rauch et al. (1991) determined $T_{\rm eff} = 75$kK, log $g = 5.0$, $n_{\rm H}/n_{\rm He} = 2$, $n_{\rm N}/n_{\rm He} = 0.006$, and $n_{\rm C}/n_{\rm He} = 0.012$. However, for none of these stars an associated PN is detected.

Thus, the evolutionary status of O(He) type CSPN is not really understood: The photospheric abundances of K 1-27 (Paper I) and LoTr 4 indicate that they could be "born-again post-AGB stars" according to the evolutionary scenario of Iben et al. (1983) and Iben & MacDonald (1995): In late stages of post-AGB evolution the photospheric abundances of C, N, and O increase rapidly while the former hydrogen-rich and most of the helium-rich envelopes are ejected. H 1504+65 (Werner 1991) is the most extreme example for a very late stage within this scenario: it has presumably lost totally its entire hydrogen and helium-rich envelopes and exhibits now the naked C-O core. It is possible that the O(He) stars represent the other "extreme", i.e. these objects are still in a mass-loss phase which will strip off H and He from their surface and then they will become PG 1159 stars in their later evolution. LoTr 4's position close to the [WC] - PG 1159 transition objects A 30 and A 78 (Leuenhagen et al. 1993, Werner & Koesterke 1992) and close to Longmore 4 whose central star experienced recently a spectacular mass-loss event (Werner et al. 1992) may even suggest this. However, a direct evolution into a DO white dwarf can not be excluded.

We note that LoTr 4 is located within the GW Vir instability strip (Werner et al. 1995a). The fact that LoTr 4 is non-variable (Bond et al. 1993) is most probably a consequence of the very low C and O abundances, because Starrfield et al. (1984) have shown that high amounts C and O are necessary to drive the pulsations in PG 1159 stars.

From our nebula analysis firm conclusions can be made: The total ionized nebula mass is about $M_{\rm ion} = 0.29\,M_\odot$, which is quite "normal", compared to that of K 1-27 ($M_{\rm ion} = 0.018\,M_\odot$, Paper I). The nebula helium abundance of LoTr 4 is definitely "normal" within 0.05 dex, and there is no stratification of the He/H abundance ratio. The heavy elements seem to be within 0.1 dex solar.

However, this is not in contradiction with a super-wind phase (Iben et al. 1983, Sect. 1) as predicted in the "born-again scenario": if we assume that LoTr 4 is a "born-again post-AGB" star at a distance of about 6 kpc (with a corresponding nebula radius of 0.6 pc) with an average nebula expansion velocity of 20 km/sec, we calculate an expansion time of 29000 ± 12000 years. The present position of LoTr 4 in Fig. 1 of Wood & Faulkner (1986) indicates a time < 300 years since its second ("born-again") departure from the AGB. Thus, material ejected since the late He flash occurred (at $T_{\rm eff} \gtrsim 100$ kK, Fig. 1 of Wood & Faulkner 1986) is still located in the inner hundredth ($<0.4''$, Sect. 1, Fig. 3) of the nebula and thus not to resolve with ground-based telescopes.

Acknowledgements. We thank D. Koester for a detailed introduction and support in the data reduction with the IRAF software package, and R. Napiwotzki, who took the '94 spectrum of LoTr 4 and carried out its data reduction. Computations were carried out on CRAY computers (Kiel, Berlin) and Sun workstations (Kiel). This research was supported by the DFG under grants We 1312/2-3 (TR), He 1487/13-1 (JK), We 1312/6-1 (KW), and by the BMFT under grants 50 OR 9302 4 (KW) and 50 OR 9409 1 (TR).

References

Acker A., Stenholm B., Tylenda R., Raytchev B. 1991, A&AS 90, 89
Acker A., Ochsenbein F., Tylenda R., Marcout J., Schohn C. 1992, Strasbourg-ESO Catalogue of galactic planetary nebulae
Allen C.W. 1973, Astrophysical Quantities, The Athlone Press, London
Blöcker T., Schönberner D. 1990, A&A 240, L11
Bond H.E., Ciardullo R., Kawaler S.D. 1993, Acta Astron. 43, 425
Borkowski K.J., Tsvetanov Z., Harrington J.P. 1993, ApJ 402, L57
Chu Y.H. 1989, in: Torres-Peimbert S.(ed.) Planetary Nebulae, IAU Symp. 131 , Kluwer, Dordrecht, p. 105
Dimitrijević M.S., Sahal-Bréchot S. 1992, A&AS 93, 359
Dreizler S., Werner K., Heber U. 1995, in: D. Koester, K. Werner (eds.) White Dwarfs, Proc. 9th European Workshop, Springer, Berlin, p. 160
Fredrick L.W., West R.M. 1984, A&AS 56, 325
Heber U., Hunger K., Jonas G., Kudritzki R.P. 1984, A&A 130, 119
Holmberg E.B., Lamberts A., Schuster H.E., West R.M. 1978, A&AS 34, 285
Hummer D.G., Mihalas D. 1988, ApJ 331, 794
Husfeld D. 1986 Ph. D. thesis, Universität München
Iben I.Jr., MacDonald J. 1995, in: Koester D., Werner K. (eds.) White Dwarfs, Proc. 9th European Workshop, Springer, Berlin, p. 48
Iben I.Jr., Kaler J.B., Truran J.W., Renzini A. 1983, ApJ 264, 605
Köppen J. 1979, A&AS 35, 111
Lang K.R. 1980, Astrophysical Formulae, Springer, Heidelberg, p. 335ff
Leuenhagen U., Koesterke L., Hamann W.-R. 1993, Acta Astron. 43, 329
Longmore A.J., Tritton S.B 1980, MNRAS 193, 521
Méndez R.H. 1991, IAU Symp. 145, Kluwer, Dordrecht, p. 375
Moore C.E. 1971, NSRDS–NBS 3, Section 4
Moore C.E. 1980, NSRDS–NBS 3, Section 9
Pauldrach A., Puls J., Kudritzki R.P., Méndez R.H., Heap S.R. 1988, A&A 207, 123
Press W.H., Teukolsky S.A., Vetterling W.T., Flannery B.P. 1992, Numerical Recipes, 2nd ed., Cambridge University Press
Rauch T., Werner K. 1995, in: D. Koester, K. Werner (eds.) White Dwarfs, Proc. 9th European Workshop, Springer, Berlin, p. 186
Rauch T., Heber U., Hunger K., Werner K., Neckel T. 1991, A&A 241, 457
Rauch T., Köppen J., Werner K. 1994, A&A 286, 543 (Paper I)
Schönberner D. 1983, ApJ 272, 708
Schöning T. 1995, in: D. Koester, K. Werner (eds.) White Dwarfs, Proc. 9th European Workshop, Springer, Berlin, p. 113
Schwarz H.E., Corradi R.L., Melnick J. 1992, A&AS 96, 23
Starrfield S., Cox A.N., Kidman R.B., Pesnell W.D. 1984, ApJ 281, 800
Tody D. 1986, in: Crawford D.L. (ed.) Proc. SPIE 627, 733
Warmels R.H. 1991, "The ESO-MIDAS System", in Astronomical Data Analysis Software and Systems I , ASP Conference Series, Vol. 25, p. 115
Werner K. 1986, A&A 161, 177
Werner K. 1991, A&A 251, 147
Werner K. 1993, in: Barstow M.A. (ed.) White Dwarfs: Advances in Observation and Theory. NATO ASI Series C, Vol. 403, p. 67
Werner K. 1995, A&A in press
Werner K., Koesterke L. 1992, in: Heber U., Jeffery C.S. (eds.) Proc. Kiel/CCP7 Workshop, Atmospheres of Early-Type Stars. Lecture Notes in Physics, Springer, Berlin, p. 288
Werner K., Heber U., Hunger K. 1991, A&A 244, 437
Werner K., Hamann W.-R., Heber U., Napiwotzki R., Rauch T., Wessolowski U. 1992, A&A 259, L69
Werner K., Dreizler S., Heber U., Rauch T. 1995a, in Astrophysics in the Extreme Ultraviolet, IAU Colloquium 152, Cambridge University Press, in press
Werner K., Dreizler S., Heber U., et al. 1995b, A&A in press
Wood P.R., Faulkner D.J. 1986, ApJ 307, 659

This article was processed by the author using Springer-Verlag LaTeX A&A style file version 3.